Developmental Biology 428 (2017) 204–214

Contents lists available at ScienceDirect

Developmental Biology

journal homepage: www.elsevier.com/locate/developmentalbiology

Original research article

A novel technique to combine and analyse spatial and temporal expression datasets: A case study with the sea anemone *Nematostella vectensis* to identify potential gene interactions

Amir M. Abdol[a], Eric Röttinger[b], Fredrik Jansson[a,1], Jaap A. Kaandorp[a,*]

[a] Computational Science Lab, University of Amsterdam, Science Park 904, 1098 XH Amsterdam, The Netherlands
[b] Université Côte d'Azur, CNRS, INSERM, Institute for Research on Cancer and Aging (IRCAN), Nice, France

ARTICLE INFO

Keywords:
Gene regulatory networks
Spatiotemporal gene expression analysis
Reverse engineering gene regulatory networks
In situ hybridization (ISH)
qPCR gene expression
Cluster analysis

ABSTRACT

Understanding genetic interactions during early development of a given organism, is the first step toward unveiling gene regulatory networks (GRNs) that govern a biological process of interest. Predicting such interactions from large expression datasets by performing targeted knock-down/knock-out approaches is a challenging task. We use the currently available expression datasets (*in situ* hybridization images & qPCR time series) for a basal anthozoan the sea anemone *N. vectensis* to construct continuous spatiotemporal gene expression patterns during its early development. Moreover, by combining cluster results from each dataset we develop a method that provides testable hypotheses about potential genetic interactions. We show that the analysis of spatial gene expression patterns reveals functional regions of the embryo during the gastrulation. The clustering results from qPCR time series unveils significant temporal events and highlights genes potentially involved in *N. vectensis* gastrulation. Furthermore, we introduce a method for merging the clustering results from spatial and temporal datasets by which we can group genes that are expressed in the same region and at the time. We demonstrate that the merged clusters can be used to identify GRN interactions involved in various processes and to predict possible activators or repressors of any gene in the dataset. Finally, we validate our methods and results by predicting the repressor effect of *NvErg* on *NvBra* in the central domain during the gastrulation that has recently been confirmed by functional analysis.

1. Introduction

Since the last decade, the sea anemone *Nematostella vectensis* has become a popular model to study bilaterian evolution, development and more recently also regeneration (Darling et al., 2005; Layden et al., 2016). Although *N. vectensis* belongs to the Cnidaria (sea anemone, coral, "jellyfish", *Hydra*), the sister group of bilaterian animals, its gene content and genomic organization presents important similarities with the ones from vertebrates (Martindale et al., 2004; Putnam et al., 2007; Schwaiger et al., 2014). Spatial gene expression analysis has further suggested a potential functional conservation between cnidarians and bilaterians of certain genes in germ layer formation, morphogenetic movements, axial patterning and neurogenesis (Fritzenwanker et al., 2007; Layden et al., 2010; Leclère and Rentzsch, 2014; Lee et al., 2007; Marlow et al., 2009; Martindale et al., 2004; Matus et al., 2006; Rentzsch and Technau, 2016; Scholz and Technau, 2003; Wikramanayake et al., 2003). The development of functional tools has subsequently fostered a more in-depth investigation of those predictions (Genikhovich et al., 2015; Layden et al., 2012; Layden and Martindale, 2014; Leclère et al., 2016; Leclère and Rentzsch, 2014; Magie et al., 2007; Marlow et al., 2012; Rentzsch et al., 2008; Röttinger et al., 2012; Saina et al., 2009; Sinigaglia et al., 2013) including first experimental wirings of gene regulatory networks underlying germ layer formation, morphogenetic movements of gastrulation (Amiel et al., 2015; Röttinger et al., 2012), axial patterning (Genikhovich et al., 2015), sensory organ formation (Amiel et al., 2015; Sinigaglia et al., 2013) as well as neurogenesis (Layden et al., 2016). The relatively simple morphology of the embryo/larva, the tractable morphogenetic movements of gastrulation was used in a detailed cell-based model of gastrulation (Tamulonis et al., 2011). Finally, the abundance of gene expression patterns organized in a database (Ormestad et al., 2011) have also fostered computational approaches toward analysis and inferring gene regulatory networks underlying gastrulation movements by processing *in situ* hybridization images (Botman et al., 2016, 2014).

* Corresponding author.
E-mail addresses: a.m.abdol@uva.nl (A.M. Abdol), eric.rottinger@unice.fr (E. Röttinger), J.A.Kaandorp@uva.nl (J.A. Kaandorp).
[1] Present address: Centrum Wiskunde & Informatica (CWI), Science Park 123, 1098 XG Amsterdam, The Netherlands.

http://dx.doi.org/10.1016/j.ydbio.2017.06.004
Received 14 February 2017; Received in revised form 28 April 2017; Accepted 2 June 2017
Available online 08 June 2017

Inferring or reverse-engineering spatiotemporal gene regulatory networks is the approach of determining gene interactions in order to reproduce the observed spatiotemporal gene expression patterns. The pioneering work by Mjolsness and Reinitz proposed a mathematical model, *Connectionist Model of Development*, capable of reproducing the gene expression patterns in space and time (Mjolsness et al., 1991). Thereafter, based on high-quality data collected during early development of *Drosophila melanogaster*, the gap gene network was constructed by fitting the model to the data (Jaeger et al., 2004; Reinitz and Sharp, 1995). This reverse-engineered gene regulatory network has then been used to explain the formation of gap genes patterns in great detail and suggested slight modifications to the well investigated network obtained from functional data (Ashyraliyev et al., 2008; Jaeger et al., 2004; Perkins et al., 2006; Surkova et al., 2008).

Collecting spatiotemporal data at the level of accuracy and detail (*e.g.*, data available for *D. melanogaster*) that allows successful reverse-engineering of GRN is an organism-related (*e.g.*, synchronized and stereotyped development) and a labor-intensive task requiring a community that defines minimal standards. Unfortunately, similar high-quality datasets available for other organisms are sparse, unprocessed (*e.g.*, in the form of raw microscopy images) or collected using methods (*e.g.*, *in situ* hybridization) that are less suitable for quantification. In the case of the sea anemone *N. vectensis*, Botman and colleagues extracted the expression patterns of several genes from *in situ* hybridization images (Botman, 2012) available in the Kahi Kai gene expression database (Ormestad et al., 2011). Subsequently, the authors applied the same mathematical model and reverse-engineering approach used for *D. melanogaster* in order to infer the underlying GRN involved in the gastrulation process of *N. vectensis* (Botman et al., 2014). However, the constructed network could not entirely reproduce the experimental data from chosen genes consist of *NvTwist*, *NvFoxA* and *NvSnail* (Botman et al., 2014) for the following reasons: limited number of temporal and spatial data points available (only two spatial patterns for each gene), uncertainty in the selected GRN and complex nature of reverse-engineering biological networks.

In this paper, we introduce a method to enrich the spatial gene expression information extracted from *in situ* hybridization images like the data available for *N. vectensis,* by combining it with quantitative information provided by qPCR measurements over time. Additionally, we show that the in-depth cluster analysis of each data type (*in situ* and qPCR) leads to better understanding of dominant regions of the embryo and temporal events during development, respectively. Furthermore, we introduce a new method to merge *in situ* and qPCR clusters together, in order to better identify possible gene interactions in different developmental stages. Finally, we discuss how our method and results can be used to reconstruct a GRN involved in a specific process and to guide biologists to design more accurate and focused experiments.

2. Material and method

Based on published spatial expression patterns extracted from *in situ* hybridization images of *N. vectensis* available in the public expression database Kahi Kai (Ormestad et al., 2011), as well as fine-scale temporal expression (qPCR) (Röttinger et al., 2012; Amiel et al., submitted), we have created two internal datasets that were optimized and used for further processing. Our temporal gene expression dataset provides quantitative information about the *relative expression level* of a gene at several time points during early embryonic development of *N. vectensis*. Yet, it does not contain any spatial information about where exactly genes are expressed in the embryo. On the other hand, our spatial gene expression dataset (Botman et al., 2016) consists of extracted spatial expression patterns of genes from *in situ* hybridization images (Botman, 2012) which do not provide a quantitative estimate of gene expression level. Therefore, our temporal and spatial expression datasets, each captures a different aspect of gene expression. Here we demonstrate that the cluster analysis of each dataset separately reveals valuable information about distinct developmental processes and regions of the embryo. Moreover, we introduce a method for linking temporal and spatial clusters together; then, we will discuss that the analysis of linked clusters could resolve ambiguity appeared in individual clusters and also provide testable hypotheses.

2.1. Processing qPCR Data

Quantitative real-time polymerase chain reaction, qPCR, is a well-established and accurate laboratory method for measuring the concentration of a specific gene product by estimating its mRNA. Most qPCR experiments use a control gene, *house-keeping* gene, to be able to calculate the relative concentration of a selected gene. The same principle makes it possible to calculate the fold change of a gene between two (or more) experiments, developmental stages or consecutive time points during the development. In order to compute the fold changes of a gene in time, we adopted a method introduced by Pfaffl as follow (Pfaffl, 2001). First, the average Ct values of all replicates, if any, are being computed at each time-point, $\overline{Ct}_i$; then, the difference between $\overline{Ct}$ at $t = 0$ and $t = i$ will be measured as $\Delta\overline{Ct}_i = \overline{Ct}_i - \overline{Ct}_0$. Finally, by having the *amplification factor* of each gene, ϵ^g, we could compute the fold change of mRNA templates at each time-point, $E_i^g = (\epsilon^g)^{-\Delta\overline{Ct}_i}$. As mentioned, if the house-keeping gene is shared between experiments, then the normalized fold change of a gene with respect to its house-keeping gene can be computed using the efficiency of the house-keeping gene, $F_i^g = E_i^g/\epsilon_i^{\text{house-keeping gene}}$.

A dataset of qPCR measurements of over 200 genes from early developmental stages of *N. vectensis* has been collected, studied and published by Röttinger et al. (2012), Amiel et al. (submitted). Each gene is measured in 3 replicates, in 16 time-points: 0, 2, 4, 6, 8, 10, 12, 14, 16, 18, 20, 24, 28, 32, 40, 48 hour post fertilization, *hpf*; from early unfertilized eggs to late gastrulation stage using *NvActin* as the house-keeping gene. We calculated the fold changes of all genes in the dataset; also, we applied several data processing routines to the dataset in order to *deal with missing data, interpolate the intermediate points* and to *normalize the fold change*. It is important to mention that *normalized fold changes* can be used to compare temporal dynamics of genes with each other during the development; however, they should not be considered as quantitative measurements. Fig. 1 shows the processing

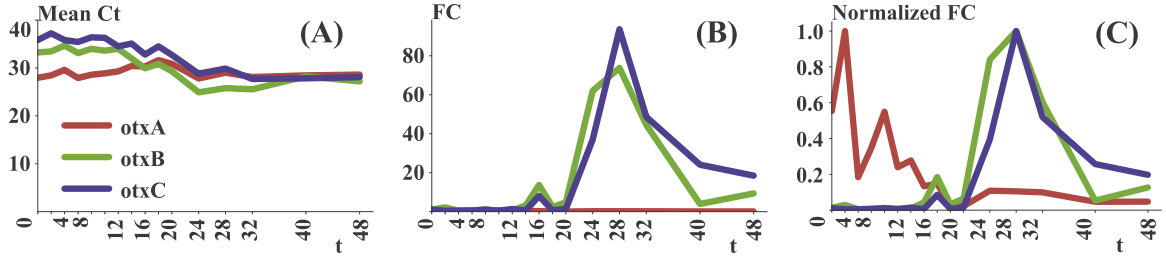

Fig. 1. From qPCR Ct values to normalized Fold Change. (A) $\overline{Ct}$ of *NvOtxA*, *NvOtxB*, *NvOtxC* genes. (B) Relative fold changes with respect to *NvActin* house-keeping gene. (C) Normalized fold change of *NvOtx*'s family.

steps toward computing the normalized fold change of *NvOtx* genes family.

2.2. Processing expression patterns extracted from in situ images

Among several methods available for studying spatial gene expression, *RNA in situ hybridization* and *protein immunolocalization* techniques are the most commonly used methods to detect the expression territory of a gene. However, one of the main drawbacks of this method is the fact that the *in situ* images do not provide accurate quantitative information about gene expression. In fact, while the colour intensity of the staining can vary in regard to the gene expression level, other factors such as staining duration, staining method and imaging technique (*e.g.*, chemical *vs.* fluorescent) can drastically influence the final results (Botman, 2012; Botman et al., 2014).

Despite the mentioned drawbacks, recent studies introduced a method for computationally extracting spatial gene expression information from *in situ* hybridization images of *N. vectensis* (Botman, 2012; Botman et al., 2014). Botman manually selected the outlines of ectoderm and endoderm of embryos in each image, then removed the background colour and measured the colour intensity along the marked area thus providing spatial expression level of genes in the embryo, (Botman et al., 2014 (Fig. 5.)). They also considered the length variations between different embryos by using percentages to represent embryo's length where x-axis correspond to length of the embryo and $x_{i+1} - x_i$ is equivalent to 1% of embryo and both $x = 0$ and $x = 100$ correspond to *apical pole* and $x = 50$ is located in *oral pole*, as illustrated later in the text in Fig. 4(A, C). In the rest of this text, we use the same representation.

Although Botman et al. (2014) implemented several filters and post-processing steps to accurately extract the expression patterns from an image (Botman, 2012), the extraction of gene expression profiles from *N. vectensis* embryo's stayed a challenging task. Their method is still very sensitive to the quality of the image, light source, hybridization details and accurate detection of cells layer. Alternation in the latter often results in slight variations in peaks position extracted from the same *in situ* image. Additionally, due to the non-synchronous nature of *N. vectensis* development, *hour post fertilization* (*hpf*) is normally a rough indication of developmental stages. In fact, previous work has shown that a variation of up to 35% in the number of cells at a given time point during early development can be observed within a batch of "synchronously" fertilized oocytes (Röttinger et al., 2012). Thus, morphologically distinguishing *in visu* of a 18 h blastula from a 21 h blastula is usually a difficult task and also has to take into account the culturing temperature. This could also lead to variation or fluctuation in spatial gene expression pattern.

In order to reduce the uncertainty induced by the data and the extraction method, we produced three internal datasets of *in situ* expressions extracted from the same set of images available to us where each can be considered as different replicates reflecting the fluctuations in the extraction algorithm, Fig. 2(A). Here, we calculated the average expression pattern from all different measurements available, Fig. 2(B). Moreover, we estimated the missing spatial pattern between two available patterns when it is possible; for instance, in the case of *NvBra*, spatial data is available at 14, 24, 28 and 40*hpf* but not at 18*hpf*. We used *linear interpolation* to estimate the missing spatial pattern as shown in Fig. 2 with the green filled pattern at *late blastula* stage.

2.3. Constructing continuous spatiotemporal gene expression levels

Here we introduce a method to combine two datasets with each other. As discussed, the qPCR data is quantitative but *in situ* expressions are not. Thus, we will combine the quantitative information from temporal data to spatial data extracted from *in situ* hybridization images. To do so, we will adjust the expression level of spatial patterns using the qPCR fold change of a gene over developmental time.

2.3.1. Time synchronization

In situ expression patterns are usually labelled according to developmental stages of *N. vectensis* which can be translated to a window of time after fertilization which itself depends on the raising temperature. In contrast, available qPCR experiments are performed more precisely, and the values are reported at specified hour post fertilization similarly in regard to the raising temperature. In order to merge the datasets, we need to estimate the duration of each developmental stage and also match and synchronize the times and stages between the two datasets. Table 1 lists time intervals for each developmental stage of *N. vectensis* embryos that were cultured at 17 °C (Ormestad et al., 2011).

Based on the approximate duration of each stage, we associated every *in situ* image to an exact *hpf* within the selected time interval. For instance, an expression domain identified in an early blastula will be associated to 12*hpf* at 17 °C. For relatively short developmental stages (less than 4 h), we have used the starting time and for longer stages, we approximately take the middle point. These assumptions are only being used in the following section and it will not affect the clustering results.

2.3.2. Adjusting the spatial expression level by qPCR data

It is important to emphasize that F_i^g indicates the relative changes in expression of a gene at $t = i$ relative to its value at $t = 0$, in the whole organism. In addition, the area under the extracted spatial pattern, a 1D curve, is also relatively representative of total expression of a gene detected in the organism although as discussed it is not quantitative. Therefore, we can use qPCR fold change value to relatively adjust the height of a spatial pattern to its relative gene expression level as indicated by qPCR fold change. For example, if F_{12}^g indicates the fold change of a gene at $t = 12$ then the area under the spatial pattern in early blastula (eb), P_{eb}^g, has to be scaled to have the area equal to F_{12}^g, or $\int P_{eb}^g(x)dx = F_{12}^g$. Fig. 3(B) shows the adjusted expression level of *NvBra* at different developmental stages using this method. Notice that the height of spatial curves corresponds to the height of qPCR fold change at the same time. In this case, we could see a high gene expression level of *NvBra* at early blastula in *central domain/rings*; then, the expression level drops but the gene expression pattern stays in the *oral ectoderm* during gastrulation at relatively stable levels, Fig. 3.

In the presence of a sufficient number of spatial expression profiles in different stages or time-points through the course of development, we are able to extend the adjustment method to estimate the continuous spatial and temporal expression pattern of a gene. Here we used *linear interpolation* to estimate the spatial pattern of a gene at time points where qPCR measurements are available. Thereafter, we are able to apply the expression level adjustment procedure, as discussed in the previous section, to each intermediate pattern and construct the *continuous spatiotemporal expression levels* of a gene during the development. For example, Fig. 3(C) shows the estimated spatial expression pattern of *NvBra* during development where we estimated the spatial patterns at every 1 h and adjusted the area under each curve to its corresponding qPCR fold change value.

It is important to state that using *linear interpolation* for estimating intermediate spatial expression profiles may lead to erroneous conclusions due to the possible nonlinear regulation of a gene or/and morphological changes of the embryo in the course of early development. However, in case of *NvBra* we argue that provided enough prior knowledge about gene's behaviours, the reconstructed expression profile could be informative and it is in agreement with its proposed behaviour (Kraus and Technau, 2006).

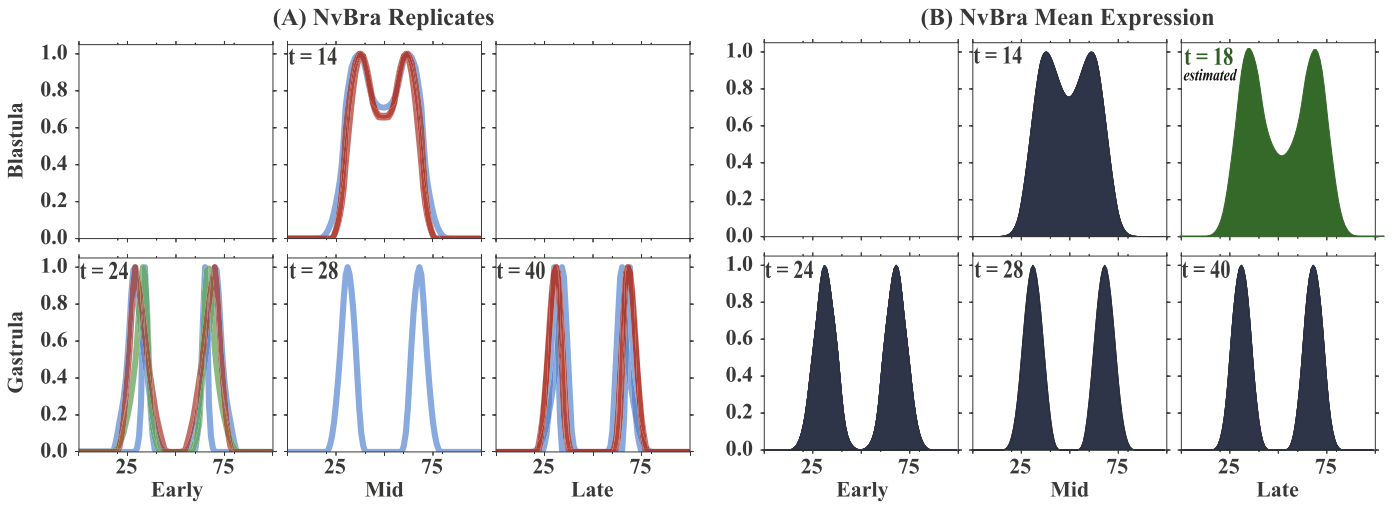

Fig. 2. Raw and processed spatial expression patterns of *NvBra* from early blastula to late gastrula stage. (A) Extracted expression patterns of *NvBra*. Each colour represents the data from each of our internal dataset. (B) Aggregated and normalized gene expression. The green pattern at late blastula stage is an estimated pattern, Section 2.3.2. Filling has been used only for clarification of *adjustment method*, Section 2.3.2.

Table 1
Each row indicates one developmental stage of *N. vectensis* with its used abbreviation mentioned in parenthesis.

Developmental Stage	*Hpf* Interval	*Hpf* Reference
Zygote (zy)	(0, 2)	1
Cleavage (cl)	(2, 12)	8
Early Blastula (eb)	(12, 14)	12
Mid Blastula (mb)	(14, 18)	14
Late Blastula (lb)	(18, 20)	18
Early Gastrula (eg)	(20, 28)	24
Mid Gastrula (mg)	(28, 32)	28
Late Gastrula (lg)	(32, 50)	40
Early Planula (ep)	(50, 60)	55
Mid Planula (mp)	(60, 70)	65
Late Planula (lp)	(70, 80)	75

Hpf Interval, hour post fertilization, indicates the start and end of each interval and the *Hpf* Reference used as a reference time for a specific stage for organisms cultured at 17 °C.

3. Results

Clustering methods are commonly used for identifying genes groups that share similar characteristics. However, clustering results have to be interpreted cautiously since they could depend on both the robustness of clustering algorithm as well as the property of the data. For instance, although clustering *in situ* expressions could identify groups of genes with similar spatial patterns, genes in one cluster might not be expressed at the same time. On the other hand, because *in situ* expression usually are not quantitative, the clustering algorithm has no information over the actual expression level of genes, and this could lead to clustering genes together that are not necessarily have similar levels of expression or temporal dynamics. In contrast, clustering time-series, *e.g.*, qPCR, ideally groups of genes that are possibly active at the same time or following similar temporal dynamic; however, since qPCR does not provide any spatial information, genes in one cluster might not be present at the same regions in the embryo. In fact, with no prior knowledge of genes, it is risky to conclude gene interactions or functions solely based on their appearance together in either of the clusters individually. In the reminder of this section, we take a different approach toward clustering by linking clusters from each data source together; then, we show that the analysis of linked clusters could resolve ambiguity appeared in individual clustering and also provide testable hypotheses. A similar approach has been used for identification of syn-expressed genes by classification of fused microarray and *in situ* image data of *D. melanogaster* embryo (Costa et al., 2007).

In order to optimize the robustness of our clustering results, we have mainly used *KMeans* clustering method for both temporal and spatial data (Pedregosa et al., 2012). Due to the sensitivity of *KMeans* algorithm on the initial guess for the number of clusters, we have used the *Silhouette* score to measure the consistency of *KMeans* for different values of K (The silhouette score lays between [−1, 1] where higher value indicates that members of each cluster are tightly grouped together). We estimated the upper bound of K by visually inspecting a dendrogram diagram constructed using average linkage as a dissimilarity measure and the Euclidean distance as a meter. Thereafter, we ran the silhouette analysis over *KMeans* results for $K = 1 \ldots 2N$ (N: number of prominent clusters in dendrogram) by calculating the

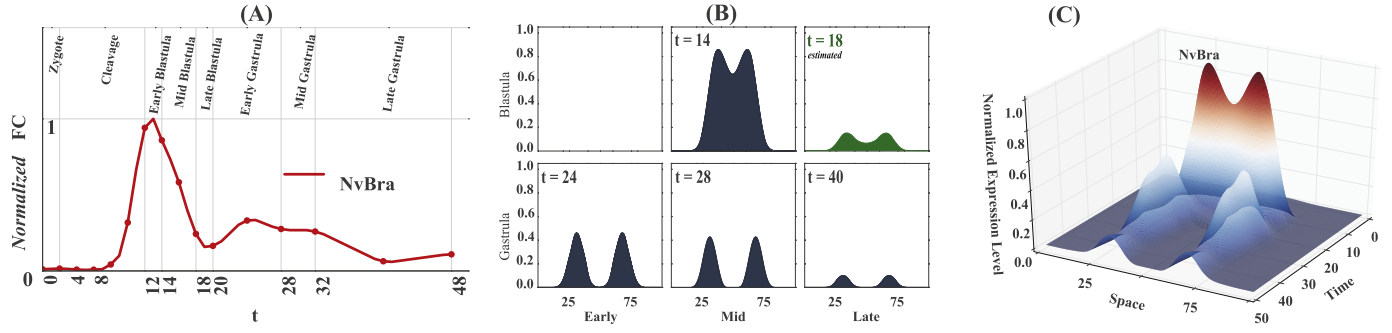

Fig. 3. Adjusting spatial gene expression patterns with qPCR fold change. (A) *NvBra* normalized qPCR fold change, the change in expression can be seen in each developmental stage. (B) Scaled spatial expression patterns of *NvBra* using the normalized fold change at each developmental stage. Filling illustrates the relation between the area under the *in situ* curve and the qPCR fold change. (The green pattern at late blastula stage is an estimated pattern, Section 2.3.2.) (C) Approximated continuous relative spatial expression pattern of *NvBra*.

overall silhouette score and producing the silhouette plot. Then, we selected a K with highest overall score as long as the "thickness" and contribution of each cluster to overall score are relatively similar. Finally, we have performed the same procedure with different random seeds in order to check the consistency of our results. In the rest of this section, we report the *silhouette score* of every cluster presented.

3.1. Clustering in situ expression patterns

Here we are interested in identifying dominant regions of the embryo in each distinct developmental stage as well as identifying genes that belong to each region. As mentioned, the *KMeans* clustering algorithm is applied on all *in situ* expression patterns in order to cluster genes with similar spatial patterns as well as identifying the centroids of each cluster which are defined as the mean of all members in each cluster. Due to significant morphological changes of the embryo from *blastula* to *gastrula*, we divided the *in situ* expressions into two categories based on the developmental stage from which they originated. *In situs* between 12 and 20 *hpf* are assigned to *blastula* stage, and those from 20 to 50 *hpf* are assigned to *gastrula* stage. This eliminates the possible effects of abrupt changes in gene expression patterns due to morphological changes of the embryo. Dividing the *in situ* expressions into two separate categories also improves the quality of our clustering results since the algorithm could distinguish genes with different spatial patterns in *blastula* and *gastrula* and therefore, assigning them to different clusters if they change their expression regions from one stage to another.

Fig. 4(B) shows the centroid of each cluster at blastula stage. It is important to emphasize that each centroid is a representative of a group of genes in our spatial expression dataset. Our cluster analysis identified four dominant expression regions during blastula stage (silhouette score: 0.56). With the assumption that the overall number of cells does not change drastically from early to late blastula stage, peaks in the middle and two ends of the x-axis are most likely establishing the *central domain* and *apical domain* regions of the embryo, respectively. Expression peaks in between them, are establishing regions known as *central rings* and *external rings* which later in the development together, most likely, form the future *pharynx* of the organism.

Fig. 4(D) shows cluster centroids during the *gastrulation* stage. We identified six dominant expression patterns during *gastrulation* (silhouette score: 0.55). Due to the more complex morphology of embryo at the *gastrula* stage, the assignment of peaks to their corresponding regions is less accurate than for the *blastula* stages. For instance, **green** peak corresponds to *body wall endomesoderm*. From three central symmetrical peaks, (**red** – **orange** - **blue**), the **blue** peak may correspond to *oral ectoderm*, and although distinguishing the **red** and **orange** peaks and assigning them to their corresponding regions is more challenging, they may correspond to the *pharyngeal ectoderm* and the *pharyngeal endomesoderm*, respectively. **Purple** peaks are probably corresponding to *body wall ectoderm* and **brown** peaks are corresponding to *apical* and (or) *sub-apical poles*. At both stages, our identified dominant gene expression regions are in agreement with

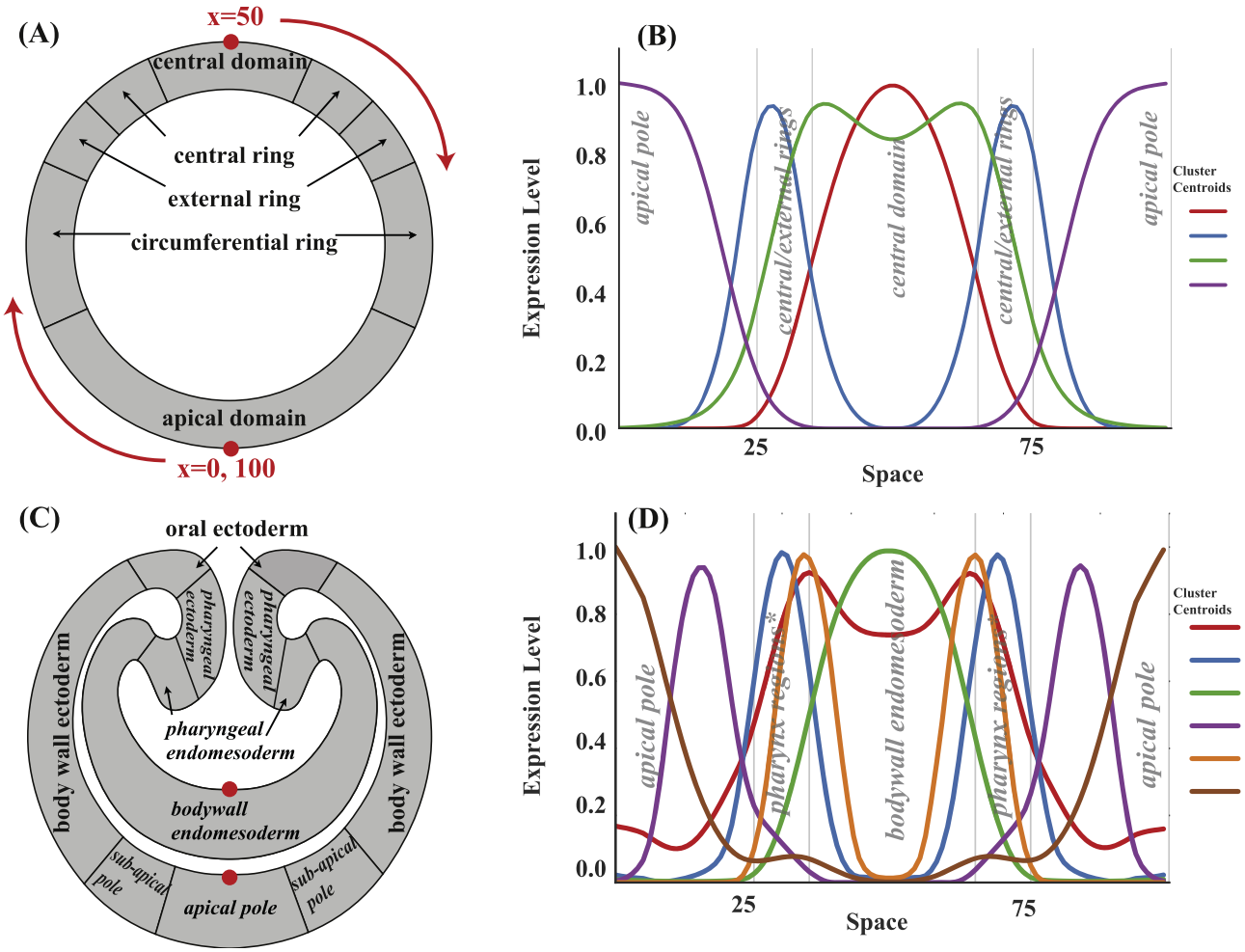

Fig. 4. Dominant expression regions of *N. vectensis* embryo during *blastula* and *gastrula* stages identified by cluster centroids. (A) Schematic representation of the embryo at blastula stage with suggested regions. (B) Clustering centroids appears at important regions of the embryos during the blastula. (C) Schematic representation of the embryo at gastrula stage (Pharynx consist of three distinct regions: body wall endomesoderm, pharyngeal endomesoderm and pharyngeal ectoderm). (D) Clustering centroids appears at important regions of the embryos during the gastrula.

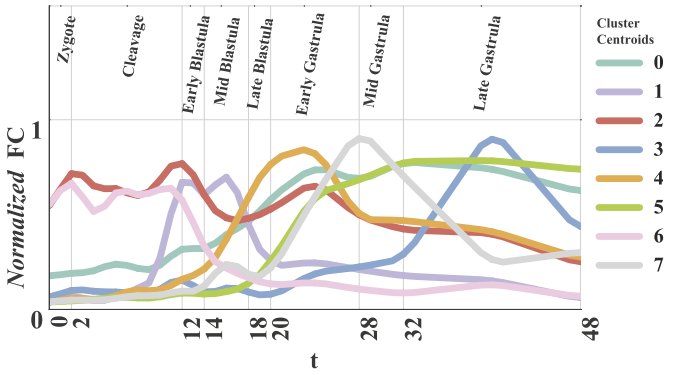

Fig. 5. Cluster centroids from clustering normalized fold changes. Eight different cluster centroids have been detected each indicating possible temporal event during the early developmental process in *N. vectensis*. Genes in each cluster are listed in Table 2.

published observations (Röttinger et al., 2012; Amiel et al., submitted). Genes belong to each cluster can be found in Figs. 6 and 7 where they have been coloured accordingly.

3.2. Clustering qPCR fold change

The same clustering method can be applied to qPCR measurements to identify genes with similar temporal dynamics. The *KMeans* clustering results are not as robust as clustering results of spatial expression patterns (silhouette score: 0.25) which mean genes loosely belong to their clusters. However, it is still possible to identify dominant temporal dynamics (cluster centroids) during the development. As Fig. 5 shows, eight dominant temporal dynamics are identified. Two groups of genes are more expressed during the cleavage stage, genes in **2** and **6** clusters; however, the remaining genes have relatively low expression and they are starting to be expressed during early blastula stage. Following the temporal dynamics towards blastula stage in Fig. 5, we see that genes classified as **2** and **6** are being less expressed during blastula stages despite their relatively higher expression levels in the previous stage. Moreover, genes categorized as **1** are starting to be more expressed while the rest of genes are still having stable but low level of expression. At the end of the blastula stage, we could observe higher expression of cluster **0, 4, 5, 7,** which were fairly inactive prior to this stage. Finally, genes in cluster **3** are being more expressed at later stages of gastrulation. Table 2 shows the list of genes in each cluster.

3.3. Analysis of combined spatial and temporal clusters

Here we propose a method to combine and interpret clusters from *in situ* expressions and qPCR fold changes together. Figs. 6 and 7 are showing instances of combined clusters. In order to construct a network in Fig. 6, for example network **B**, we start by selecting all genes that belong to temporal expression cluster 1 (root id in network **B**) from Table 2. We then remove genes with no spatial information available for them; and finally, we colour the remaining genes according to the *in situ* clusters that they belong to in Fig. 4. Therefore, the node (*i.e.* gene name) colors indicate which *in situ* cluster a gene belongs to (spatial information, Fig. 4) and the edge (lines connecting the genes) colors imply what qPCR cluster a gene is originating from (temporal information, Fig. 5). Therefore, we could interpret each network as a group of genes appearing in the same region in the embryo (according to spatial clusters, Fig. 4) and with a relatively similar level of gene expression at the same time (based on qPCR clusters, Fig. 5). Later, we will discuss how this information can be used to identify similar or dissimilar genes at each developmental stage.

4. Discussion

We showed that the analysis of qPCR dataset could reveal different temporal events during the development as well as suggesting genes involved in each process. As shown in Fig. 5, one or more cluster centroids are suggesting distinct temporal events during development. Cluster **2** and **6** are strongly suggesting a family of genes that are expressed/active during cell divisions period and becoming less active afterward. Cluster **1** indicates the preparation of embryo for the formation of the blastula. In addition, distinct events at every stage of gastrulation can be predicted by clusters **4**, **7** and **3** respectively. Overall, different cluster centroids are suggesting distinct chronological events during the developments. Some of the predicted events are in agreement with already known results, for instance, Röttinger and colleagues suggested the initiation of a bulk zygotic gene expression or *mid-blastula transition* (MBT) (Röttinger et al., 2012). They have suggested that *N. vectensis* goes through an MBT-like event during early *blastula* (10 *hpf*). Our data agrees with their theory by showing the rise in the expression level of a cluster of genes just before the start of the *blastula* (~10 *hpf*).

Similarly, we showed that results from *in situ* clustering would lead to conclusions about dominant expression regions in the embryo in different developmental stages. They can also be used to identify or track the expression regions of a specific gene. As an example, Fig. 4(B) and Fig. 6(B) show that *NvBra (N. vectensis Brachyury)* belongs to the **green** cluster during *blastula* (expressed in the *central domain* with

Table 2
Known genes in each qPCR cluster.

id	Genes
0	arntl-like, ax1/hoxf, cad-c, cad-e, cad-f, cappucino-like, cubulin-like1, dhand, ets-like, fgfr-like, foxa, foxd3, foxq2-like3, hox2, klf5-like, klf7-like, mab21-like2, nfkb, porcupine-l, rx1, sfrp1/5-like, sox10-like, sp8/9-like, tbx15, vegfr-like, wnt3, wnt7b
1	ashb, bra, duxabc, evx, fgfra, foxa/b-like, foxb, fz10, hd017, hd032, hd043, hd065, hd147, hes1-like, hes3, lhx1, lhx6, moxc, msxa, msxb, ncam3, nvduxabc, nvhd017, snaila, snailb, twist, wnt1, wnt2, wnt8, wnt8b
2	actin, atonal-like, axin-like, creb-like, fgf20-like, fgfr-l2, fgfrb, hd050, hd052, mab21-like3, nk2-like, pr2-like, shavenbaby-like, smad1/5, smad4, smad4-like, vasa1
3	ax1a, ax8, blimp1, cordin, cv2, dkk-like3, dkk3-like1, dmbxc, dmbxf, elka-like, fgf8/17-like, fix/nfi, gata, gcm, hd007, hd077, hex, hrtl-like, kielin-like, lim, lim1-like, meis, nkd1-like, tbx1, vasa2, wnt16
4	delta, dkk124, ehand-like, elk-like, erg, eve, follistatin-like, fosb-like, foxq1-like, foxq2, gdf5, hd067, hlxb9, ikb, mae-like, maf-like, musk-like, nanos1, neurod, q50-6 (hd145), rfp-like, six3/6, sprouty, stra, tbx20-like2, wnt11, wnta
5	bicaudal, c-myc-like, cad-g, coup1-like, dlx, fgfrc, fox1, foxd1, foxj1-like, fz1-like, gfi-like, glis, gsc, hbp1-like, hd037, hd058, not1 (hd145), hes-like1, hes-like2, hes-like5, hes2, hex1, hmx3, k50-5, mae, miwi-like, paxa, pea3-like, perlecan-like, pl10, pn5, pou-like1, pou-like2, pou-like3, repo, rx3-like, sox2, tolloid, vegf-like2, vsx-like, wnt5, wnt6
6	activin, ax6a, bcl2-like, admp-related, bmp5/8, elav-like, hd056, hd060, hh1, nanos2, onecut-like, otxa, pdef-like, phtf1-like, ret-like2, snip1-like, soxb1, tbx18-like, tcf, tela-like, vasa-like, vcam1-like, vegf-like, vent2
7	ax1, bmp1-like, bmp2/4, cad-a, cad-b, coup-like2, fgf1a, fgf2a, fgf8a, gli, hd010, moxd, ncam1, nk-like13, nk2a-like, otxb, otxc, rfx4-like, runt, six4/5, tailless-like, tolloid-like, wnt4

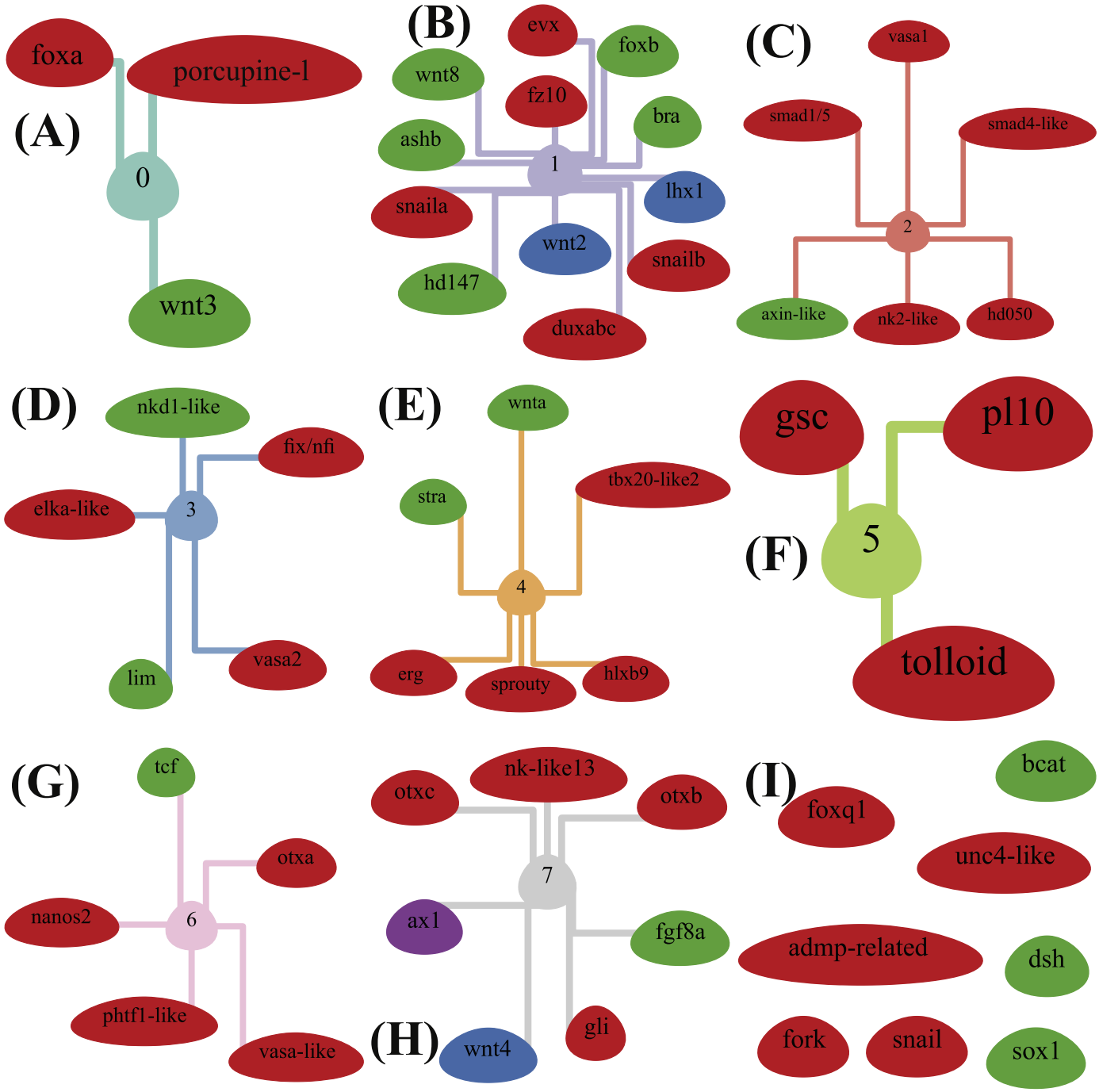

Fig. 6. Combined qPCR and *in situ* clusters during blastula stage. From A to I, the root numbers and colors refer to qPCR clusters (Fig. 5) and node colors refer to *in situ* clusters (Fig. 4(B)), respectively. For genes with no root, qPCR data were not available.

higher peaks at *central ring*). However, it is part of the **blue** cluster during gastrulation (expressed in the *pharynx* regions, *i.e. pharyngeal endomesoderm* , *pharyngeal ectoderm* and *oral ectoderm*). The same behaviour is observed in orthologue of *Brachyury* in the *Sea Urchin* during the *gastrulation* process (Gross and McClay, 2001) and has been proposed to have the same behaviour in *N. vectensis* (Kraus and Technau, 2006).

Additionally, we introduced a method for combining clusters of *in situ* and qPCR data. Figs. 6 and 7 provide a unique categorization of data in time and space distinguished by developmental stage. In Fig. 8, we have provided a guideline on how to predict possible interactions between genes in each stage from Figs. 6 and 7. Cumulatively these predictions will lead to the construction of GRN candidates involved in certain processes. For example, by assuming that the gastrulation process initiates after formation of three distinct expression regions at blastula stage (*central domain*, *central/external ring* and *apical domain*) (Botman, 2012; Botman et al., 2014), we can start selecting genes that are active in the mentioned regions before and during the formation of blastula. Therefore, from networks **A, B, C, E, G** in Fig. 6, *NvFoxA*, *NvSnailA*, *NvSnailB, NvOtxA*, *NvNanos2, NvErg* (genes in **red**) and *NvBra*, *NvFoxB*, *NvWntA*, *NvTcf* (genes in **green**) are good candidates for genes concentrated in *central domain* and *central ring respectively*. *NvLhx1* and *NvWnt2* (genes in **blue**) are good candidates for genes concentrated in *central/external rings* and finally *NvAx1* (genes in **purple**) is the only candidate for genes concentrated in *apical regions*. Interestingly, we see similar expression regions for

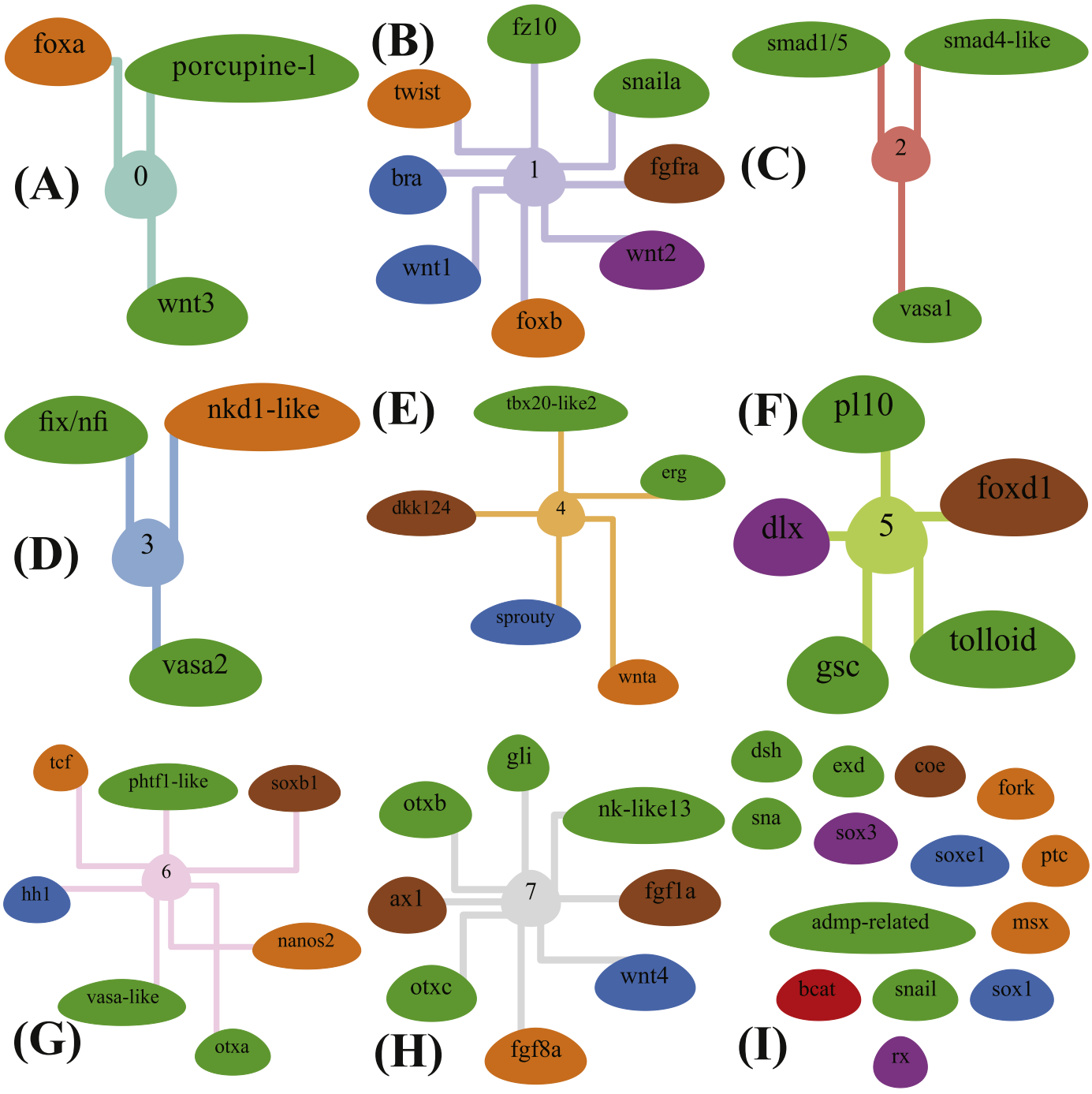

Fig. 7. Combined qPCR and *in situ* clusters during gastrula stage. From A to I, the root numbers and colors refer to qPCR clusters (Fig. 5) and the node colors refer to *in situ* clusters (Fig. 4, (D)), respectively. For genes with no root, qPCR data were not available.

NvSnailA and *NvFoxA* during *blastula*. However, looking further into *gastrulation* (Fig. 7), we see the complementary expression of *NvFoxA* and *NvSnailA*. This has been observed by Magie and colleagues that performed two colors *in situ* hybridization of *NvFoxA* and *NvSnailA* (Magie et al., 2007). Moreover, our selected list of genes consists of several known genes involved in gastrulation in other organisms; for instance, as suggested the repressor function of *Snail* is necessary for *Drosophila* gastrulation (Hemavathy et al., 2004).

Until now, we only selected genes that are spatially separated. This means that the genes from the two groups are either not directly interacting with each other (they are not located at the same region) or one group inhibits the expression of the other group in the same region. Latter would result in dominant expression of the inhibitor group in that region. However, we will show that it is possible to derive less trivial conclusions about gene behaviours as well. For instance, as shown in Fig. 3, the expression region of *NvBra* disappears from *central domain* during *late blastula* and concentrates more in *pharynx regions* during the *gastrulation*. Due to the complexity of *gastrulation* process, identifying the exact reason for this slight change in expression region of *NvBra* is still subject to more research. However, as observed, cells in *central/external rings* tend to move to future *pharynx* during the early gastrulation (Magie et al., 2007). This, together with the possible slow decay in concentration of *NvBra* in the *central domain/ring* leads to a visible change in expression of *NvBra*. However, if morphological factors play a minor role, repression of *NvBra* expression in *central domain/ring* by another gene will similarly lead to the

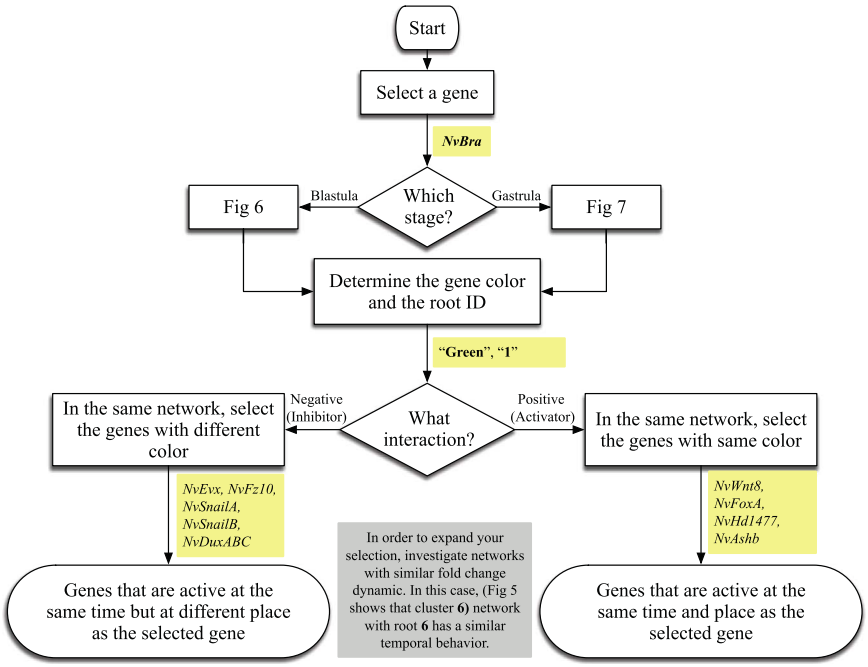

Fig. 8. Procedure to select possible activators or inhibitors of a selected gene in a selected developmental stage from Figs. 6 or 7. Yellow boxes are representing outputs of each step starting from *NvBra* as a target gene.

disappearance of *NvBra* from *central domain* at *late blastula*. We think the change in expression region is driven by both factors. The cell movement is possibly playing a major role in centralizing the expression in *pharyngeal regions*, on the other hand, not all cells from the *central domain/ring* will move to *pharyngeal regions*. Therefore, we think the expression in the *central domain* is being repressed by one or more genes during the transition from *blastula* to *gastrula*.

Here we describe in details how our combined clustering method can suggest possible inhibitors of *NvBra* during the transition from blastula to gastrula, as outlined in Fig. 9. Starting from Fig. 6, we see a possible correlation between *NvBra*, *NvFoxB*, *NvWnt8, NvHd147, NvAshB* (network **B**). In fact, they start to be expressed just before *blastula* and they are spatially restricted to the *central ring* (same colour, same root id). On the other hand, as mentioned, Fig. 7 shows that *NvBra* tends to be expressed in the *oral ectoderm* or *pharyngeal ectoderm* during the gastrulation process (moving from **green** to **blue** cluster in Fig. 4(B, D)). This suggests repression of *NvBra*, before and during the gastrulation stage, in the *central domain* by another gene (which should be activated before or at the same time) to reduce *NvBra* expression in the *central domain*. In order to find possible candidates with negative effects on *NvBra* at the start of gastrulation, we need to look at clusters **1**, **2** or **6** of Fig. 5 which consists of active genes during this stage or cluster **0** and **4** which are genes that are starting to have higher expression (activity) just before the start of gastrulation process. Checking the list of genes in clusters **0**, **1**, **2**, **4** and **6** in Table 2, we see some plausible candidates: *NvSnailA*, *NvTcf*, *NvOtxA*, *NvAxin*, *NvSmad1/5*, *NvSmad4*, *NvFz10*, *NvFoxB*, *NvWnt3*, *NvErg*. The next step toward filtering out our choices is to find the genes that are present in the *central domain* during the *gastrulation*. By identifying the colour of selected genes in Fig. 7 and knowing that genes in **green** are expressed in the *central domain*, we can narrow down our choices to *NvOtxA*, *NvSnailA*, *NvFz10*, *NvFoxB*, *NvWnt3, NvErg* as candidates for repressing *NvBra* in *central domain* during the transition from blastula to gastrula stage. A recent functional study in *Nematostella vectensis* confirms part of our prediction. In fact, inhibition of *NvErg* using a morpholino-based knockdown approach extends *NvBra* expression from the *central ring* toward the *central domain* showing that indeed, *NvBra* is actively repressed by *NvErg* in the *central domain* (Amiel et al., submitted). The other predicted potential repressors of *NvBra* need to be tested in the future.

At this point, using the information provided in Figs. 6 and 7 and following the instructions in Figs. 8 and 9, we can validate our method further by comparing our predictions to the current known GRNs of *N. vectensis* during the early-blastula and early-gastrula (Leclère et al., 2016; Röttinger et al., 2012, Amiel et al., submitted). In the case of *NvTcf,* while our method could not precisely suggest the direction of repression effect found in functional studies, we can observe the similar repression effect between *NvTcf* and *NvSnailA* at the *central/external/circumferential rings* (appearing in the **blue** and **orange** clusters (Fig. 4(B, D))). Similarly, the repression effects between *NvTcf* and *NvDuxABC, NvFgf8A, NvHlxB9* at the *central rings, central rings,* and *central/external rings* (appearing in the **red, red** and **orange** clusters in Fig. 4(B, D)) respectively. In contrast, we can observe activation effects between *NvTcf* and *NvBra, NvAsh, NvFoxB, NvWnt8* at the *central/external rings* during the late-blastula (all appearing in the **green** cluster in Fig. 4B). In the case of *NvErg,* in addition to the repression of *NvBra* by *NvErg* (in the *central domain*), we can suggest activation of *NvOtxB* and *NvOtxC* by *NvErg* in the *central domain* as well. In summary, despite the fact that our predictions lack the precise direction for the interaction, we can suggest similar interactions for genes available in our datasets and literature.

Through several examples, we showed the advantages of our methods and analysis. We showed that given the spatial and temporal gene expression datasets, we could extract the specific type of data encoded into each dataset individually. As we showed, analysis of temporal data could potentially reveal hidden temporal events in the course of development, which could be hard to identify only from experiments. Additionally, with analysis of spatial data we were able to reveal important regions in the embryo with possibly different functional properties. Finally, our multi-layered cluster analysis can produce testable hypothesis about possible gene interactions, reveal non-trivial behaviours of a gene, and predict GRNs controlling certain developmental processes. Additionally, in Materials and Methods section, we presented a method to combine spatial and temporal data and provide a continuous representation of gene expression level in time and space through the embryonic development of *N. vectensis*; consequently, improving the quality and quantity of data for further reverse-engineering purposes.

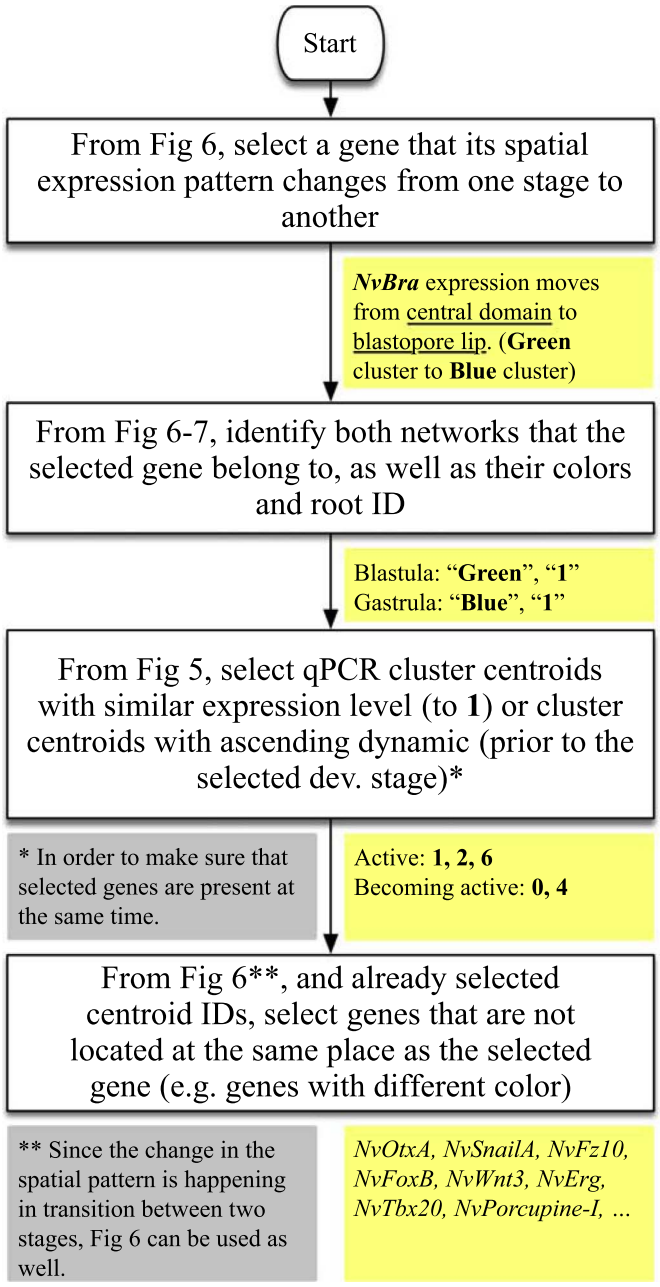

Fig. 9. Procedure to select possible activators or inhibitors of a gene during the transition between blastula to gastrula stage. Yellow boxes are representing outputs of each step starting from *NvBra* as a target gene.

Given the scalability and independency from a type of organism and prior knowledge on biological functions of genes, our method can be used to analyse large spatial and temporal datasets of other organisms in order to reveal distinct developmental events, identify important regions and hypothesize about possible gene interactions. Results from our method can also be used to design more accurate experiments by guiding biologists to focus on particular time, region or genes that could significantly improve accuracy and reduce experimental costs. Consequently, new experimental results such as *in situ* hybridization images, qPCR measurements or a new type of data, *e.g.* RNAseq measurements, can be inserted to the datasets, leading to more refined results and analysis of gene interactions and behaviours.

Funding

AMA: This work was supported by the EU project BioPreDyn (EC FP7-KBBE-2011-5, grant number 289434) and Swarm-Organ project (Seventh Framework Programme FP7/2007–2013, grant number 601062) also MopDev project funded by Netherlands Science Foundation Complexity-Net project MOPDEV (645.100.005). FJ: Swarm-Organ. ER: ATIP-Avenir award (C13992AS) (Plan Cancer), a Marie-Curie Career Integration Grant (631665) (CIG—FP7, European Commission) as well as grants from the "Association pour la Recherche sur le Cancer (ARC)" (PJA 2014120186).

Acknowledgements

We wish to thank Eva Deutekom and Roland Dries for insightful comments, discussions and critical reading of the manuscript.

Appendix A. Supplementary material

Supplementary data associated with this article can be found in the online version at doi:10.1016/j.ydbio.2017.06.004.

References

Amiel, A.R., Johnston, H., Chock, T., Dahlin, P., Iglesias, M., Layden, M., Röttinger, E., Martindale M.Q., A bipolar role of the transcription factor ERG for cnidarian germ layer formation and apical domain patterning. (submitted).
Amiel, A.R., Johnston, H.T., Nedoncelle, K., Warner, J.F., Ferreira, S., Röttinger, E., 2015. Characterization of morphological and cellular events underlying oral regeneration in the sea anemone, Nematostella vectensis. Int J. Mol. Sci. 16, 28449–28471.
Ashyraliyev, M., Jaeger, J., Blom, J.G., 2008. Parameter estimation and determinability analysis applied to Drosophila gap gene circuits. BMC Syst. Biol. 2, 83.
Botman, D., 2012. Spatial gene expression quantification: a tool for analysis of in situ hybridizations in sea anemone Nematostella vectensis. BMC Res. Notes 5, 555.
Botman, D., Jansson, F., Röttinger, E., Martindale, M.Q., de Jong, J., 2016. Analysis of a spatial gene expression database for sea anemone Nematostella vectensis during early development. BMC Syst. Biol., 1–22.
Botman, D., Röttinger, E., Martindale, M.Q., de Jong, J., 2014. A computational approach towards a gene regulatory network for the developing Nematostella vectensis gut. PLoS One 9, e103341.
Costa, I.G., Krause, R., Opitz, L., Schliep, A., 2007. Semi-supervised learning for the identification of syn-expressed genes from fused microarray and in situ image data. BMC Bioinform. 8, S3–S15.
Darling, J.A., Reitzel, A.R., Burton, P.M., Mazza, M.E., Ryan, J.F., Sullivan, J.C., Finnerty, J.R., 2005. Rising starlet: the starlet sea anemone, Nematostella vectensis. BioEssays 27, 211–221.
Fritzenwanker, J.H., Genikhovich, G., Kraus, Y., Technau, U., 2007. Early development and axis specification in the sea anemone Nematostella vectensis 310, 264–279.
Genikhovich, G., Fried, P., Prünster, M.M., Schinko, J.B., Gilles, A.F., Fredman, D., Meier, K., Iber, D., Technau, U., 2015. Axis patterning by BMPs: cnidarian network reveals evolutionary constraints. Cell Rep. 10, 1646–1654.
Gross, J.M., McClay, D.R., 2001. The role of brachyury (T) during gastrulation movements in the sea urchin Lytechinus variegatus. Dev. Biol. 239, 132–147.
Hemavathy, K., Hu, X., Ashraf, S.I., Small, S.J., Ip, Y.T., 2004. The repressor function of snail is required for Drosophila gastrulation and is not replaceable by Escargot or Worniu. Dev. Biol. 269, 411–420.
Jaeger, J., Surkova, S., Blagov, M., Janssens, H., Kosman, D., Kozlov, K.N., Manu, Myasnikova, E., Vanario-Alonso, C.E., Samsonova, M., Sharp, D.H., Reinitz, J., 2004. Dynamic control of positional information in the early Drosophila embryo. Nature 430, 368–371.
Kraus, Y., Technau, U., 2006. Gastrulation in the sea anemone Nematostella vectensis occurs by invagination and immigration: an ultrastructural study 216, 119–132.
Layden, M.J., Boekhout, M., Martindale, M.Q., 2012. Nematostella vectensis achaete-scute homolog NvashA regulates embryonic ectodermal neurogenesis and represents an ancient component of the metazoan neural specification pathway. Development 139, 1013–1022.
Layden, M.J., Martindale, M.Q., 2014. Non-canonical Notch signaling represents an ancestral mechanism to regulate neural differentiation. EvoDevo 5, 30–14.
Layden, M.J., Meyer, N.P., Pang, K., Seaver, E.C., Martindale, M.Q., 2010. Expression and phylogenetic analysis of the zic gene family in the evolution and development of metazoans. EvoDevo 1, 12.
Layden, M.J., Rentzsch, F., Röttinger, E., 2016b. The rise of the starlet sea anemone Nematostella vectensis as a model system to investigate development and regeneration. Wiley Interdiscip. Rev.: Dev. Biol., (n/a–n/a).
Leclère, L., Bause, M., Sinigaglia, C., Steger, J., Rentzsch, F., 2016. Development of the aboral domain in Nematostellarequires β-cateninand the opposing activities of Six3/6and Frizzled5/8. Development 143, 1766–1777.

Leclère, L., Rentzsch, F., 2014. RGM regulates BMP-mediated secondary axis formation in the sea anemone Nematostella vectensis. Cell Rep. 9, 1921–1930.
Lee, P.N., Kumburegama, S., Marlow, H.Q., Martindale, M.Q., Wikramanayake, A.H., 2007. Asymmetric developmental potential along the animal–vegetal axis in the anthozoan cnidarian, Nematostella vectensis, is mediated by Dishevelled. Dev. Biol. 310, 169–186.
Magie, C.R., Daly, M., Martindale, M.Q., 2007. Gastrulation in the cnidarian Nematostella vectensis occurs via invagination not ingression. 305, 483–497.
Marlow, H., Roettinger, E., Boekhout, M., Martindale, M.Q., 2012. Functional roles of Notch signaling in the cnidarian Nematostella vectensis. Dev. Biol. 362, 295–308.
Marlow, H.Q., Srivastava, M., Matus, D.Q., Rokhsar, D., Martindale, M.Q., 2009. Anatomy and development of the nervous system of Nematostella vectensis, an anthozoan cnidarian. Dev. Neurobiol. 69, 235–254.
Martindale, M.Q., Pang, K., Finnerty, J.R., 2004. Investigating the origins of triploblasty: `mesodermal' gene expression in a diploblastic animal, the sea anemone Nematostella vectensis (phylum, Cnidaria; class, Anthozoa). Development 131, 2463–2474.
Matus, D.Q., Pang, K., Marlow, H., Dunn, C.W., Thomsen, G.H., Martindale, M.Q., 2006. Molecular evidence for deep evolutionary roots of bilaterality in animal development. Proc. Natl. Acad. Sci. USA 103, 11195–11200.
Mjolsness, E., Sharp, D.H., Reinitz, J., 1991. A connectionist model of development. J. Theor. Biol. 152, 429–453.
Ormestad, M., Martindale, M.Q., Röttinger, E., 2011. A comparative gene expression database for invertebrates. EvoDevo 2, 17.
Pedregosa, F., Varoquaux, G., Gramfort, A., Michel, V., Thirion, B., Grisel, O., Blondel, M., Louppe, G., Prettenhofer, P., Weiss, R., Dubourg, V., Vanderplas, J., Passos, A., Cournapeau, D., Brucher, M., Perrot, M., Duchesnay, É., 2012. Scikit-learn: Machine Learning in Python. arXiv.
Perkins, T.J., Hallett, M., Glass, L., 2006. Dynamical properties of model gene networks and implications for the inverse problem. BioSystems 84, 115–123.
Pfaffl, M.W., 2001. A new mathematical model for relative quantification in real-time RT-PCR. Nucl. Acids Res. 29, e45.
Putnam, N.H., Srivastava, M., Hellsten, U., Dirks, B., Chapman, J., Salamov, A., Terry, A., Shapiro, H., Lindquist, E., Kapitonov, V.V., Jurka, J., Genikhovich, G., Grigoriev, I.V., Lucas, S.M., Steele, R.E., Finnerty, J.R., Technau, U., Martindale, M.Q., Rokhsar, D.S., 2007. Sea anemone genome reveals ancestral eumetazoan gene repertoire and genomic organization. Science 317, 86–94.
Reinitz, J., Sharp, D.H., 1995. Mechanism of eve stripe formation. Mech. Dev. 49, 133–158.
Rentzsch, F., Fritzenwanker, J.H., Scholz, C.B., Technau, U., 2008. FGF signalling controls formation of the apical sensory organ in the cnidarian Nematostella vectensis. Development 135, 1761–1769.
Rentzsch, F., Technau, U., 2016. Genomics and development of Nematostella vectensis and other anthozoans. Curr. Opin. Genet. Dev. 39, 63–70.
Röttinger, E., Dahlin, P., Martindale, M.Q., 2012. A framework for the establishment of a cnidarian gene regulatory network for "endomesoderm" specification: the inputs of ß-catenin/TCF signaling. 8, e1003164.
Saina, M., Genikhovich, G., Renfer, E., Technau, U., 2009. BMPs and chordin regulate patterning of the directive axis in a sea anemone. Proc. Natl. Acad. Sci. USA 106, 18592–18597.
Scholz, C.B., Technau, U., 2003. The ancestral role of Brachyury: expression of NemBra1 in the basal cnidarian Nematostella vectensis (Anthozoa). 212, 563–570.
Schwaiger, M., Schönauer, A., Rendeiro, A.F., Pribitzer, C., Schauer, A., Gilles, A.F., Schinko, J.B., Renfer, E., Fredman, D., Technau, U., 2014. Evolutionary conservation of the eumetazoan gene regulatory landscape. Genome Res. 24, 639–650.
Sinigaglia, C., Busengdal, H., Leclère, L., Technau, U., Rentzsch, F., 2013. The bilaterian head patterning gene six3/6 controls aboral domain development in a Cnidarian. PLoS Biol. 11, e1001488–16.
Surkova, S.Y., Myasnikova, E.M., Kozlov, K.N., Samsonova, A.A., Reinitz, J., Samsonova, M.G., 2008. Methods for acquisition of quantitative data from confocal images of gene expression in situ. Cell Tissue Biol. 2, 200–215.
Tamulonis, C., Postma, M., Marlow, H.Q., Magie, C.R., de Jong, J., Kaandorp, J., 2011. A cell-based model of Nematostella vectensis gastrulation including bottle cell formation, invagination and zippering. Dev. Biol. 351, 217–228.
Wikramanayake, A.H., Hong, M., Lee, P.N., Pang, K., Byrum, C.A., Bince, J.M., Xu, R., Martindale, M.Q., 2003. An ancient role for nuclear beta-catenin in the evolution of axial polarity and germ layer segregation. Nature 426, 446–450.